Superconductivity in the ferromagnetic semiconductor samarium nitride

E.-M. Anton,[1] S. Granville,[2] A. Engel,[3] S. V. Chong,[2] M. Governale,[1] U. Zülicke,[1] A. G. Moghaddam,[4] H. J. Trodahl,[1] F. Natali,[1] S. Vézian,[5] and B. J. Ruck[1,*]

[1]*MacDiarmid Institute for Advanced Materials and Nanotechnology, School of Chemical and Physical Sciences, Victoria University of Wellington, P. O. Box 600, Wellington 6140, New Zealand*

[2]*MacDiarmid Institute for Advanced Materials and Nanotechnology, Robinson Research Institute, Victoria University of Wellington, P. O. Box 33436, Lower Hutt 5046, New Zealand*

[3]*Physics Institute, University of Zürich, Winterthurerstr. 190, 8057 Zürich, Switzerland*

[4]*Department of Physics, Institute for Advanced Studies in Basic Sciences (IASBS), Zanjan 45137-66731, Iran*

[5]*Centre de Recherche sur l'Hétéro-Épitaxie et ses Applications (CRHEA), Centre National de la Recherche Scientifique, Rue Bernard Gregory, 06560 Valbonne, France*

Conventional wisdom expects that making semiconductors ferromagnetic requires doping with magnetic ions and that superconductivity cannot coexist with magnetism. However, recent concerted efforts exploring new classes of materials have established that intrinsic ferromagnetic semiconductors exist and that certain types of strongly correlated metals can be ferromagnetic and superconducting at the same time. Here we show that the trifecta of semiconducting behavior, ferromagnetism, and superconductivity can be achieved in a single material. Samarium nitride (SmN) is a well-characterized intrinsic ferromagnetic semiconductor, hosting strongly spin-ordered $4f$ electrons below a Curie temperature of 27 K. We have now observed that it also hosts a superconducting phase below 4 K when doped to electron concentrations above 10^{21} cm^{-3}. The large exchange splitting of the conduction band in SmN favors equal-spin triplet pairing with p-wave symmetry. Significantly, superconductivity is enhanced in superlattices of gadolinium nitride (GdN) and SmN. An analysis of the robustness of such a superconducting phase against disorder leads to the conclusion that the $4f$ bands are crucial for superconductivity, making SmN a heavy-fermion-type superconductor.

I. INTRODUCTION

Conventional superconductivity arises due to spin-singlet Cooper pairing of electrons into an s-wave orbital bound state [1]. While most elemental and compound superconductors are of the conventional type, alternative pairing mechanisms have attracted great interest over the years [2–4], most recently fuelled by the drive to understand the origin of high superconducting transition temperatures [5]. The fermionic nature of electrons requires that spin-singlet (spin-triplet) Cooper pairs have even (odd) orbital-bound-state angular momentum. Hence, unconventional spin-singlet (spin-triplet) superconducting order parameters can have d-wave, g-wave, etc. (p-wave, f-wave, etc.), symmetry.

The possibility to form spin-triplet Cooper-pair states underpins the coexistence of magnetism and superconductivity observed in certain bulk metals [6–10]. The same physics also enables the generation of spin-polarized supercurrents in hybrid structures of conventional (s-wave) superconductors with ferromagnets [11,12], thus opening interesting new opportunities for implementing a spin-based electronics paradigm [13] in the context of superconductivity [14–16]. The p-wave spin-triplet pairing channel has become prominent as the most likely candidate mechanism at play in real systems. Furthermore, recent interest has focused on quasi-one-dimensional p-wave superconductivity induced in *semiconductor* nanowires with strong spin-orbit coupling through proximity to an s-wave superconductor, because such hybrid systems can be driven

into a topologically nontrivial phase where they host Majorana excitations [17–20]. This last development is only the most recent advance in the long-running drive to further enhance the versatility of semiconductors' materials properties, e.g., by making them superconducting [21–23] or ferromagnetic [24–27], and thus enable the realization and exploitation of new electronic and magnetic phenomena.

Here we report the presence of superconductivity in the doped intrinsic ferromagnetic semiconductor samarium nitride (SmN), in which magnetism and superconductivity are simultaneously observed in a semiconducting material. While the coexistence of ferromagnetic order and superconductivity is in itself an interesting phenomenon, the fact that this coexistence occurs in a semiconductor offers an enhanced level of tunability and potential for novel device applications. Peculiar to SmN, the large exchange splitting of its conduction and valence bands [28] renders it very likely to harbor fully spin-polarized carriers, thus ruling out any type of spin-singlet pairing as the origin of the observed superconducting order—including the putative (Fulde-Ferrell-Larkin-Ovchinnikov) inhomogeneous scenario [29,30]. Instead, the superconducting state hosted by SmN is of an unconventional triplet type, most likely exhibiting p-wave symmetry. In addition, we find stronger superconductivity in samarium nitride/gadolinium nitride (SmN/GdN) superlattices. Since GdN is a ferromagnetic semiconductor with no propensity to become superconductive, this provides further evidence of the coexistence of superconductivity and magnetism in SmN. The results presented in this article open up new opportunities associated with the ability to control semiconducting, ferromagnetic, and superconducting properties in a single material and, in the process, access novel states of quantum matter [31].

---

*ben.ruck@vuw.ac.nz

The paper is organized as follows. In the immediately following Sec. II, the basic magnetic and electronic properties of SmN are introduced. We then provide details about the experimental techniques employed in our study in Sec. III. The main experimental results are presented in Sec. IV, showing superconductivity in thin-film SmN samples and its strengthening in SmN/GdN superlattices. Section V is devoted to a theoretical analysis of the experimental results, and we summarize the main findings of the paper in Sec. VI.

II. REVIEW OF THE MAGNETIC AND ELECTRONIC PROPERTIES OF SmN

The past decade has seen significant advances in the growth and passivation of thin films of the rare-earth nitrides LN, where L denotes a member of the lanthanide series [32–34]. In particular, it is known that almost all of them are semiconductors in both their paramagnetic and ferromagnetic states. In the same time frame, there has been progress in theoretical treatments of strongly correlated electrons that enabled reliable band-structure calculations that show good agreement with recent experimental studies [35]. The band structures predicted by the treatments show indirect band gaps, with the N $2p$ valence band (VB) maximum at Γ and the L $5d$ conduction band (CB) minimum at X. In addition, there are L $4f$ bands that cross the valence and conduction bands at energies that vary across the series. GdN, with its exactly half-filled $4f$ shell, has the majority-spin $4f$ bands about 8 eV below, and the minority-spin bands about 5 eV above the gap [28,33]. In materials involving lighter L elements, there are empty majority-spin bands threading the CB, while for LNs with heavier L elements, there are filled minority-spin bands crossing the VB. These are generally very narrow, heavy-mass bands, though they must hybridize at some level with the $2p$ and $5d$ bands.

For GdN, it is now clear that there is a finite band gap [36,37], which has facilitated this material's integration into device structures [38,39]. The available experimental data also support the presence of a finite band gap in SmN [34,35,40], although the data are less complete than for GdN and the possibility of a small band overlap cannot be ruled out at present [41]. In any case, the rare-earth nitrides commonly exhibit high carrier concentrations and metallic behavior due to large concentrations of N vacancies, which potentially release three electrons per defect [34,42,43]. The band structure of SmN is represented schematically in Fig. 1, where the metallic behavior is represented by the Fermi level E_F being located above the CB minimum [34,44]. This arrangement is consistent with the experimentally measured carrier concentration of 2×10^{21} cm^{-3} in the SmN sample showing superconductivity (see below), which corresponds to a N-vacancy concentration of a few percent.

The lanthanide (L^{3+}) ions in the nitrides have partially filled $4f$ shells which harbor the majority of the magnetic moments. However, unlike transition-metal compounds, the strong spin-orbit coupling and the relatively weak intra-ion overlap conspire to prevent a full quenching of the orbital magnetic moment. As a result, the net magnetic moment of these ions can be dominated by either the spin or orbital contribution. SmN holds a special place in the series [45]. As expected from applying Hund's rules, it has a near-zero
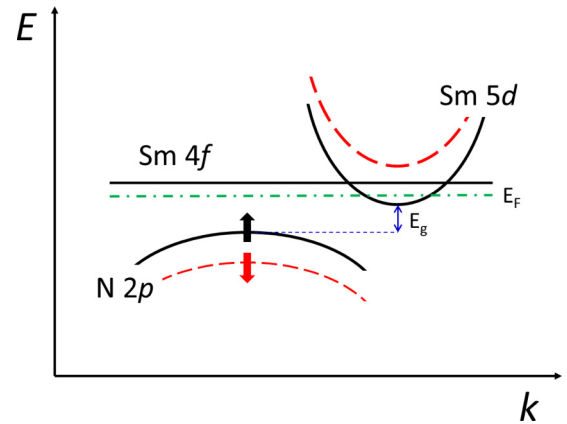

FIG. 1. Schematic representation of the band structure of SmN. The valence and conduction bands are split into majority-spin (black solid curves) and minority-spin (red dashed curves) by the exchange interaction with filled $4f$ levels. An empty majority-spin $4f$ level is shown as a dispersionless band near the conduction-band minimum. Its exact location, and the size (or even sign) of the band gap E_g, are not well known. Here the Fermi level E_F is shown inside the conduction band so the SmN is degenerately doped.

magnetic moment in the ferromagnetic phase due to an almost perfect cancellation of the $4f$ spin magnetic moment by the opposing $4f$ orbital contribution. Nonetheless, its $4f$ spins are aligned as in any ferromagnet, showing a coercive field of more than 6 T at 2 K [46,47]. The evidence for ferromagnetic alignment is unambiguous, including a clear hysteretic behavior of the magnetization, the $4f$ spin alignment measured by x-ray magnetic circular dichroism (XMCD) at the $M_{4,5}$ edges, and neutron diffraction studies [46–49]. The large $4f$-$5d$ exchange interaction then drives a large spin splitting of several hundred meV in the Sm $5d$-dominated conduction band [28]. A direct signature of that spin splitting is provided by XMCD at the Sm $L_{2,3}$ edges. These $2p$-$5d$ transitions represent spin-resolved electronic transitions into the conduction band, so their XMCD spectra are to first order proportional to the size of the spin splitting [50]. The strong XMCD signal shown in Fig. 2 confirms that the conduction band is indeed strongly spin split, and an associated hysteresis further confirms the ferromagnetic ordering of the Sm moments [47].

III. DETAILS OF EXPERIMENTAL METHODS

The films used in this study were prepared by molecular beam epitaxy in our two laboratories, at Victoria University of Wellington and at CRHEA-CNRS in Valbonne. High-purity Sm or Gd metal was evaporated in the presence of $\sim 3 \times 10^{-4}$ mbar molecular nitrogen (N$_2$), which reacts spontaneously with the metal to form the nitride. The film thicknesses of $\sim$100 nm were determined by Rutherford backscattering spectrometry. The superlattice comprised layers of 10 nm GdN and 5 nm SmN, determined with a microbalance calibrated by prior Rutherford backscattering spectrometry. The (111)-oriented epitaxial films were grown at 400−500 °C on the hexagonal face of aluminium nitride (AlN), which was in turn grown on either commercial c-plane sapphire or (111) silicon. To prevent oxidation, a 50 to 150 nm thick gallium nitride or AlN capping layer was grown on
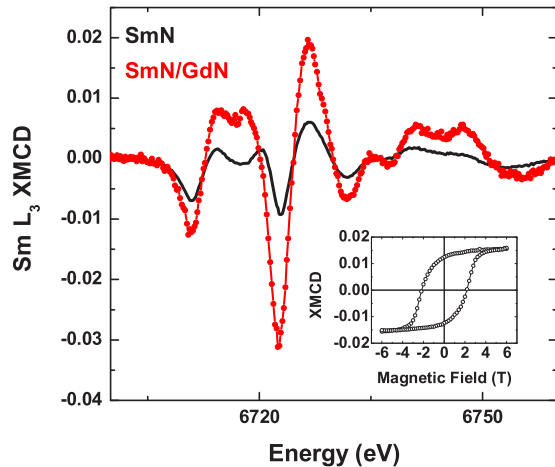
FIG. 2. X-ray magnetic circular dichroism (XMCD) at the Sm L_2 edge in a bulk SmN film and a SmN/GdN superlattice taken at 15 K and 6 T, which measures transitions into conduction-band (CB) states. The large XMCD amplitude demonstrates the strong exchange splitting between spin-up and spin-down CB states. The XMCD signal is 3 times larger in the superlattice sample (cf. Refs. [47,48]), implying an even stronger CB spin splitting in that case. The inset shows the associated magnetic hysteresis of the bulk SmN film measured using XMCD, confirming the ferromagnetism.

top of the rare-earth nitride films. Further details of the growth procedure can be found elsewhere [51,52].

The low energy of formation of nitrogen vacancies dictates that their concentration is of order 1% at the high growth temperatures used for the rare-earth nitride layers [43], but reducing the temperature yields films with lower nitrogen-vacancy doping [34]. The carrier concentration is amenable to being controlled: It can be reduced by compensating codopants (e.g., magnesium) [42] or increased by restricting the partial pressure of N_2 during the deposition of the rare-earth metal [53]. Figure 3 shows a typical temperature-dependent resistivity for a SmN sample with low nitrogen-vacancy doping. The
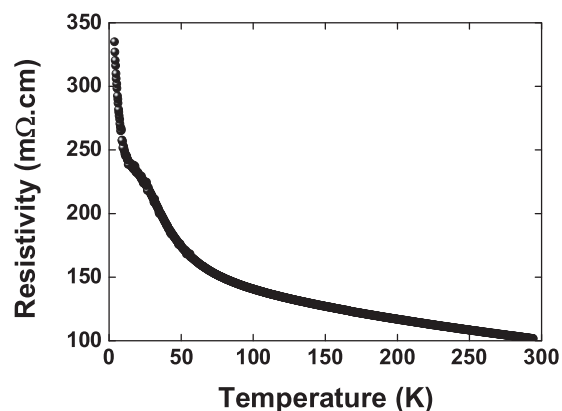

FIG. 3. The resistivity of a near-stoichiometric SmN film with low carrier concentration. In this film, the resistivity rises continuously as the temperature falls, with an anomaly at the Curie temperature signaling the development of spin splitting at the band edges. There is no sign of an onset of superconductivity in this sample.

data establish clearly that this near-stoichiometric SmN is a semiconductor, with no sign of superconductivity.

The resistivity and magnetoresistance data in Figs. 4(a) and 4(b) were measured in the van-der-Pauw geometry in perpendicular field in a Quantum Design PPMS equipped with a He-3 option. For Fig. 5(b), a PPMS with a horizontal rotator option was used to allow measurements in both parallel and perpendicular fields with respect to the plane of the film. The resistivity data in Fig. 5(a) and Fig. 3 were measured in a closed-cycle cryostat. The magnetic data were obtained with a Quantum Design MPMS-7 SQUID magnetometer. To show the diamagnetism in the superconducting state, the measurements were performed in field-normal configuration because the superconducting penetration depth is larger than the film thickness.

IV. EXPERIMENTAL RESULTS

A. Superconductivity in homogeneous SmN

While investigating electronic and magnetic properties for epitaxial films of the rare-earth-nitride series, we have found that many of our SmN films, and so far only SmN, display clear superconductivity when sufficiently heavily doped. Interestingly, the metallic, nonmagnetic end members of the rare-earth nitride series have been known to be superconducting for some time [54,55].

In Fig. 4(a) we show the temperature-dependent resistance of a homogeneous SmN film that displays the superconducting transition at low temperature and, at higher temperature, an anomaly at the Curie temperature. This film, with an electron concentration of 2×10^{21} cm^{-3}, exhibits the onset of superconductivity at 2–3 K and reaches zero resistance below 0.7 K. The magnetic-field-driven return to the normal state is complex, as seen in Fig. 4(b). Strict zero resistance is destroyed in fields as low as 10 mT, but superconductivity still persists in the majority of the film so the full return to the normal state does not occur below a field of about 4 T. Within the intermediate state, the resistivity displays hysteresis, seen clearly in the 0.4 K data in Fig. 4(b), signaling a coexistence of ferromagnetic and superconducting order parameters, at least in an intermediate mixed state.

In the magnetic measurements shown in Fig. 4(c), a clear signature of the superconducting diamagnetic response appears in the zero-field-cooled magnetization at the lowest temperatures. This supports the persistence of ferromagnetic order on entering the superconducting phase, though the very small magnetization of SmN limits the sensitivity of magnetization studies. The coexistence of ferromagnetic and superconducting order is established even more strongly by the field dependence of the magnetic moment in Fig. 4(d), where the diamagnetic response associated with the Meissner effect is evident at fields below about 5 mT. It is important to note that the diamagnetism is incomplete, corresponding to only 10% of the film being in the superconducting state. The Meissner fraction of approximately 0.1 and the broad superconducting transition suggest that superconductivity nucleates inhomogeneously such that this bulk film consists of Josephson-coupled superconducting domains [5,56]. The inhomogeneity may be associated with grain boundaries and other structural defects, or it may be of an electronic nature, associated with the random
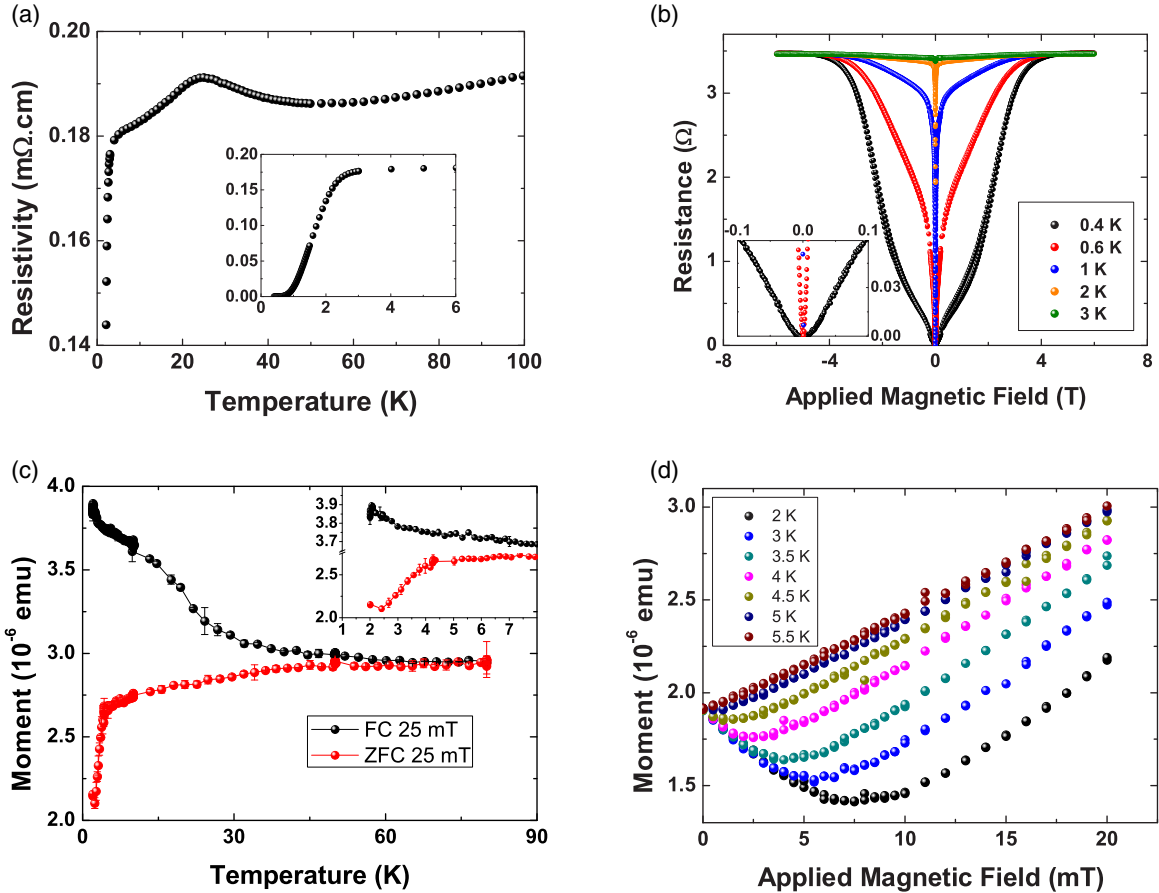
FIG. 4. (a) Temperature-dependent resistivity of a SmN film, showing an anomaly near the Curie temperature of 27 K and the onset of superconductivity below about 3 K. The inset shows the full superconducting transition. (b) Perpendicular field magnetoresistance of the sample shown in (a). (c) Field-cooled (FC) and zero-field-cooled (ZFC) magnetization data for a bulk SmN film, showing the ferromagnetic ordering that occurs below 27 K, along with evidence for the onset of superconductivity below about 4.5 K. (d) Field-dependent magnetization showing diamagnetism at low fields associated with superconductivity.

distribution of the nitrogen vacancies that provide the doping. The latter has been observed in GdN films where it leads to formation of magnetic polarons [57].

B. Superconductivity in a SmN/GdN superlattice

In order to investigate further the coexistence of superconductivity and spin-split bands, we have studied a superlattice consisting of SmN layers in direct contact with strongly ferromagnetic GdN in a $12\times(10$ nm GdN/5 nm SmN) superlattice. In this context, it is important to recognize that GdN has never shown any propensity for superconductivity. However, GdN has one of the strongest spin alignments known, with a ferromagnetically aligned $7\,\mu_B$ moment on each Gd^{3+} ion below 70 K that resides purely in its spin as the total orbital angular momentum vanishes for this half-filled $4f$ shell [34]. X-ray magnetic circular dichroism (Fig. 2) shows that the ferromagnetic exchange across the SmN/GdN interface increases the Sm $L_{2,3}$ XMCD signal by a factor of 3, i.e., the spin splitting in the conduction band of the thin SmN layers is strongly enhanced by the proximity to the ferromagnetic GdN layers [47,48].

Transport measurements shown in Figs. 5(a) and 5(b) reveal a superconducting phase that develops even more strongly in the superlattice, despite the enhanced spin splitting.

Interestingly, not only is the critical temperature higher in these layers, but also the critical field is enormously enhanced [see Fig. 5(b)], and zero resistance is maintained now to fields as large as 2 T. The coherence length implied by that critical field is ~10 nm [1], i.e., much smaller than the thickness of the homogeneous film above but comparable to the SmN-layer thickness in the superlattice. The temperature-dependent magnetization of the superlattice, shown in Fig. 5(c), is dominated by the very strong ferromagnetic moment of GdN, which has a Curie temperature of 70 K. Similarly to Fig. 4(c), Fig. 5(c) also shows a diamagnetic anomaly at the lowest temperatures, confirming the existence of the superconducting phase. Figure 5(d) displays that diamagnetic response at low fields, with a low-field slope that, in the superlattice case, corresponds to full diamagnetism (Meissner fraction of 1.0) in the SmN layers. Hence, again the superconducting signature is exhibited much more strongly in the superlattice, despite its more strongly spin-split conduction band.

V. THEORETICAL ANALYSIS: SPIN-TRIPLET HEAVY-FERMION SUPERCONDUCTIVITY

The experimental data clearly indicate a coexistence of superconductivity and ferromagnetism. The large exchange
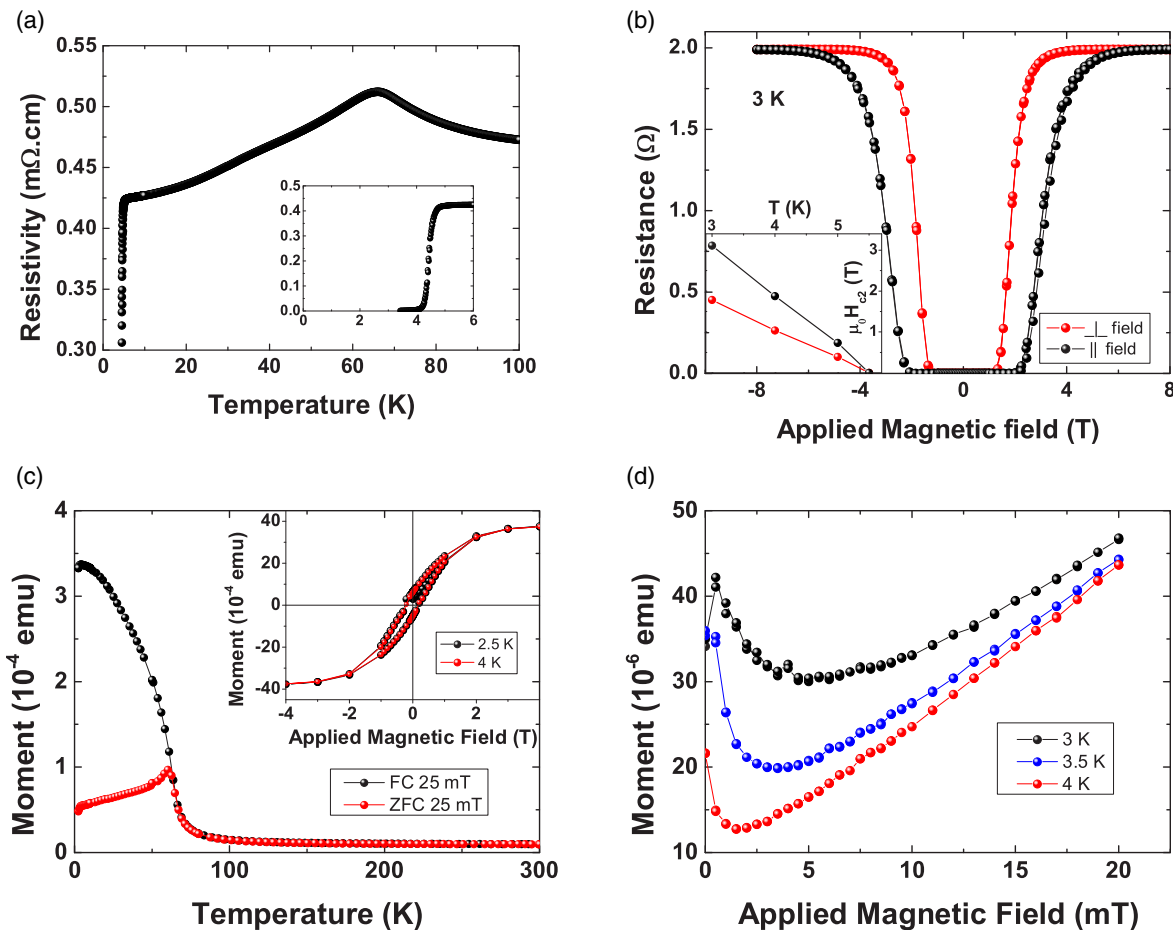
FIG. 5. (a) Temperature-dependent resistivity of a SmN/GdN superlattice, showing a much more abrupt superconducting transition than in bulk SmN films. Anomalies can be seen corresponding to the Curie temperatures of both the GdN and SmN layers, at 70 K and 30 K, respectively. (b) Magnetoresistance of the same superlattice in fields applied parallel (black) and perpendicular (red) to the layers. The line shape enables straightforward determination of an upper critical field $\mu_0 H_{c2}$. Inset: The corresponding upper critical field plotted versus temperature. (c) The temperature-dependent magnetization is overwhelmingly dominated by the GdN. Inset: Hysteresis loops confirming the GdN remains ferromagnetic even in the temperature range where the SmN is superconducting. (d) The low-field magnetization shows a clear diamagnetic response in the superconducting regime that is superimposed on the large GdN magnetic moment.

splitting of the conduction and valence bands in SmN renders it a half-metallic ferromagnetic semiconductor at the doping levels realized in our samples. As a result, only majority-spin electrons are available to form Cooper pairs, and the order parameter will be a fully polarized spin-triplet state $|\Uparrow\uparrow\rangle$. Due to the fermionic nature of electrons, the orbital part of the order parameter needs to possess odd parity in space, which implies an odd orbital-angular-momentum quantum number $l = 1, 3, \ldots$ or, using the commonly adopted atomic convention, $p, f, \ldots$ symmetry. Most probably, the lowest value of Cooper-pair angular momentum compatible with the required order-parameter symmetry will be realized, and therefore we assume a p-wave pairing. The associated pair potential $\Delta_{\uparrow\uparrow}(\mathbf{k})$ can, in principle, have the following possible states:

$$\Delta_{\uparrow\uparrow}(\mathbf{k}) = \Delta_0 \times \begin{cases} \frac{k_z}{k_F} & p_z\text{-like symmetry} \\ \frac{k_x \pm i k_y}{k_F} & p_x \pm i p_y\text{-like symmetry} \end{cases} . \quad (1)$$

For both these possibilities, the magnitude of the order parameter is given by $\Delta_0 \approx 2\hbar\Omega_c \exp(-D/\lambda)$, where D is

the number of spatial dimensions, $\hbar\Omega_c$ the cut-off energy for the attractive interaction, and λ the dimensionless coupling constant for the p-wave pairing channel. The experimental data do not give us enough information to infer the origin of the pairing interaction. However, the large splitting between majority and minority bands allows us to conclude that spin fluctuations play no role. This leaves the combination of electron-phonon and electron-electron interactions as the most likely cause for Cooper pairing in SmN. The sharper superconducting transition in the superlattice indicates a cleaner sample and/or interface-enhanced superconductivity. On the other hand, the broad superconducting transition for the thin film can be associated with the formation of domains, which is consistent with the measured incomplete diamagnetic response [see Fig. 4(d)].

An important issue for p-wave superconductivity is its weakness with respect to disorder. It has been established that, for all possible forms of the order parameter in any spatial dimension, the critical temperature T_c is suppressed with respect to the one in the absence of disorder T_{c0} according
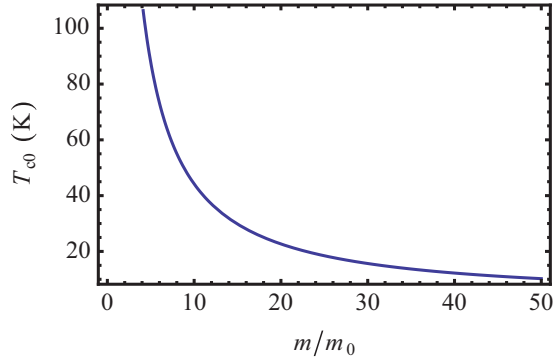
FIG. 6. Dependence of the critical temperature T_{c0} in the clean system on the superconducting charge-carriers' effective mass, m, as inferred from the measured $T_c \approx 3$ K, the normal-state resistivity, and the carrier density according to the universal theory for pair breaking in a p-wave superconductor. Here m_0 denotes the electron mass in vacuum. A highly unrealistic value for $T_{c0} \gtrsim 800$ K would be associated with the $5d$-band effective mass $m_{5d} \lesssim 0.5\,m_0$. Hence we conclude that carriers from the very weakly dispersing $4f$ band of SmN, or possibly its hybridization with the $5d$ band, must form the superconducting condensate.

to the universal formula [3]

$$\ln \frac{T_{c0}}{T_c} = \psi \left(\frac{1}{2} + \frac{\hbar}{4\pi \tau k_{\mathrm{B}} T_c} \right) - \psi \left(\frac{1}{2} \right), \qquad (2)$$

where ψ denotes the Digamma function, τ the quasiparticle scattering time, and k_{B} the Boltzmann constant. From the experimentally measured resistivity $\rho = 0.18$ mΩcm and carrier density $n = 2 \times 10^{21}$ cm^{-3} for the thin film, we can extract the scattering time τ as a function of the effective mass m by means of the Drude formula, obtaining $\tau = m/(nq^2\rho)$, where q is the electron charge. Using τ and the experimentally measured $T_c \approx 3$ K we can infer what the critical temperature would be in the absence of disorder. If we use for the effective mass a value typical for a $5d$-band $m_{5d} \lesssim 0.5\,m_0$, with m_0 being the electron mass in vacuum, we obtain a highly unrealistic value for $T_{c0} \approx 800$ K. In order to obtain a value in the realistic range $T_{c0} < 30$ K, the effective charge-carrier mass m needs to be larger than $15\,m_0$, see Fig. 6. Therefore, we must conclude that the $4f$ band is crucial for superconductivity in SmN, making it a heavy-fermion superconductor. We note at this point that such a large value for the effective mass for the quasielectrons may necessitate the consideration of nonadiabatic corrections to the electron-phonon coupling [58].

As a consistency check, we assume phonon-mediated pairing and, taking a realistic value of the Debye temperature for SmN [59] $T_D = \hbar\Omega_c/k_{\mathrm{B}} = 600$ K and an effective mass

of $m = 15\,m_0$, we find $\lambda \approx 0.8$. Such a value corresponds to a physically realistic strong coupling situation.

VI. SUMMARY AND OUTLOOK

In summary, we consistently find superconductivity below a temperature of 5 K in heavily doped ferromagnetic SmN but not in any of the other rare-earth-nitride films that we have grown. As previous work has established the unique property of SmN to have a nearly vanishing net magnetic moment coexisting with a large spin splitting in the conduction band, it can be inferred that the superconductivity resides in a majority-spin band, implying triplet pairing. SmN is further unusual in the predicted location of the very narrow majority-spin $4f$ band at the bottom of the conduction band. The full set of experimental results supports a scenario of SmN being a heavy-fermion spin-polarized superconductor with p-wave triplet pairing.

The discovery of a superconducting ferromagnetic semiconductor paves the way to explore an entirely new technological paradigm of semiconductor superspintronics. The ability to adjust the density and type of charge carriers in this material; the wide range of possibilities for integrating it into heterostructures with conventional semiconductors or other members of the rare-earth-nitride series, some of which are expected to exhibit topological order [60,61]; and the unconventional properties of p-wave superconducting phases creates a versatile platform for engineering new quantum phases of matter with potential for revolutionizing microchip design.

[1] M. Tinkham, *Introduction to Superconductivity* (McGraw-Hill, New York, 1996).

[2] M. Sigrist and K. Ueda, Phenomenological theory of unconventional superconductivity, Rev. Mod. Phys. **63**, 239 (1991).

[3] V. P. Mineev and K. V. Samokhin, *Introduction to Unconventional Superconductivity* (Gordon and Breach, New York, 1999).

[4] A. P. Mackenzie and Y. Maeno, The superconductivity of Sr$_2$RuO$_4$ and the physics of spin-triplet pairing, Rev. Mod. Phys. **75**, 657 (2003).

[5] G. Deutscher, *New Superconductors: From Granular to High T_c* (World Scientific, Singapore, 2006).

[6] S. S. Saxena, P. Agarwal, K. Ahilan, F. M. Grosche, R. K. W. Haselwimmer, M. J. Steiner, E. Pugh, I. R. Walker, S. R.

Julian, P. Monthoux, G. G. Lonzarich, A. Huxley, I. Sheikin, D. Braithwaite, and J. Flouquet, Superconductivity on the border of itinerant-electron ferromagnetism in UGe2, Nature **406**, 587 (2000).

[7] C. Pfleiderer, M. Uhlarz, S. M. Hayden, R. Vollmer, H. von Löhneysen, N. R. Bernhoeft, and G. G. Lonzarich, Coexistence of superconductivity and ferromagnetism in the d-band metal ZrZn₂, Nature **412**, 58 (2001).

[8] D. Aoki, A. Huxley, E. Ressouche, D. Braithwaite, J. Flouquet, J.-P. Brison, E. Lhotel, and C. Paulsen, Coexistence of superconductivity and ferromagnetism in URhGe, Nature **413**, 613 (2001).

[9] C. Pfleiderer, Superconducting phases of f-electron compounds, Rev. Mod. Phys. **81**, 1551 (2009).

[10] D. Aoki, F. Hardy, A. Miyake, V. Taufour, T. D. Matsuda, and J. Flouquet, Properties of ferromagnetic superconductors, Compt. Rend. Phys. **12**, 573 (2011).

[11] F. S. Bergeret, A. F. Volkov, and K. B. Efetov, Long-Range Proximity Effects in Superconductor-Ferromagnet Structures, Phys. Rev. Lett. **86**, 4096 (2001).

[12] M. Eschrig, J. Kopu, J. C. Cuevas, and G. Schön, Theory of Half-Metal/Superconductor Heterostructures, Phys. Rev. Lett. **90**, 137003 (2003).

[13] S. A. Wolf, D. D. Awschalom, R. A. Buhrman, J. M. Daughton, S. von Molnár, M. L. Roukes, A. Y. Chtchelkanova, and D. M. Treger, Spintronics: A spin-based electronics vision for the future, Science **294**, 1488 (2001).

[14] J. Linder and J. W. A. Robinson, Superconducting spintronics, Nat. Phys. **11**, 307 (2015).

[15] Matthias Eschrig, Spin-polarized supercurrents for spintronics: A review of current progress, Rep. Prog. Phys. **78**, 104501 (2015).

[16] A. C. Basaran, J. E. Villegas, J. S. Jiang, A. Hoffmann, and I. K. Schuller, Mesoscopic magnetism and superconductivity, MRS Bull. **40**, 925 (2015).

[17] R. M. Lutchyn, J. D. Sau, and S. Das Sarma, Majorana Fermions and a Topological Phase Transition in Semiconductor-Superconductor Heterostructures, Phys. Rev. Lett. **105**, 077001 (2010).

[18] Y. Oreg, G. Refael, and F. von Oppen, Helical Liquids and Majorana Bound States in Quantum Wires, Phys. Rev. Lett. **105**, 177002 (2010).

[19] V. Mourik, K. Zuo, S. M. Frolov, S. R. Plissard, E. P. A. M. Bakkers, and L. P. Kouwenhoven, Signatures of Majorana fermions in hybrid superconductor-semiconductor nanowire devices, Science **336**, 1003 (2012).

[20] A. Das, Y. Ronen, Y. Most, Y. Oreg, M. Heiblum, and H. Shtrikman, Zero-bias peaks and splitting in an Al–InAs nanowire topological superconductor as a signature of Majorana fermions, Nat. Phys. **8**, 887 (2012).

[21] T. Schäpers, *Superconductor/Semiconductor Junctions* (Springer, Berlin, 2001).

[22] T. Herrmannsdörfer, V. Heera, O. Ignatchik, M. Uhlarz, A. Mücklich, M. Posselt, H. Reuther, B. Schmidt, K.-H. Heinig, W. Skorupa, M. Voelskow, C. Wündisch, R. Skrotzki, M. Helm, and J. Wosnitza, Superconducting State in a Gallium-Doped Germanium Layer at low Temperatures, Phys. Rev. Lett. **102**, 217003 (2009).

[23] X. Blase, E. Bustarret, C. Chapelier, T. Klein, and C. Marcenat, Superconducting group-IV semiconductors, Nat. Mater. **8**, 375 (2009).

[24] T. Jungwirth, J. Sinova, J. Masek, J. Kucera, and A. H. MacDonald, Theory of ferromagnetic (III,Mn)V semiconductors, Rev. Mod. Phys. **78**, 809 (2006).

[25] Tomasz Dietl, A ten-year perspective on dilute magnetic semiconductors and oxides, Nat. Mater. **9**, 965 (2010).

[26] T. Dietl and H. Ohno, Dilute ferromagnetic semiconductors: Physics and spintronic structures, Rev. Mod. Phys. **86**, 187 (2014).

[27] T. Jungwirth, J. Wunderlich, V. Novák, K. Olejník, B. L. Gallagher, R. P. Campion, K. W. Edmonds, A. W. Rushforth, A. J. Ferguson, and P. Němec, Spin-dependent phenomena and device concepts explored in (Ga,Mn)As, Rev. Mod. Phys. **86**, 855 (2014).

[28] P. Larson, W. R. L. Lambrecht, A. Chantis, and M. van Schilfgaarde, Electronic structure of rare-earth nitrides using the LSDA + U approach: Importance of allowing $4f$ orbitals to break the cubic crystal symmetry, Phys. Rev. B **75**, 045114 (2007).

[29] P. Fulde and R. A. Ferrell, Superconductivity in a strong spin-exchange field, Phys. Rev. **135**, A550 (1964).

[30] A. I. Larkin and Y. N. Ovchinnikov, Nonuniform state of superconductors, Sov. Phys. JETP **20**, 762 (1965).

[31] Editorial, The rise of quantum materials, Nat. Phys. **12**, 105 (2016).

[32] C. M. Aerts, P. Strange, M. Horne, W. M. Temmerman, Z. Szotek, and A. Svane, Half-metallic to insulating behavior of rare-earth nitrides, Phys. Rev. B **69**, 045115 (2004).

[33] Chun-Gang Duan, R. F. Sabirianov, W. N. Mei, P. A. Dowben, S. S. Jaswal, and E. Y. Tsymbal, Electronic, magnetic and transport properties of rare-earth monopnictides, J. Phys.: Condens. Matter **19**, 315220 (2007).

[34] F. Natali, B. J. Ruck, N. O. V. Plank, H. J. Trodahl, S. Granville, C. Meyer, and W. R. L. Lambrecht, Rare-earth mononitrides, Prog. Mater. Sci. **58**, 1316 (2013).

[35] A. R. H. Preston, S. Granville, D. H. Housden, B. Ludbrook, B. J. Ruck, H. J. Trodahl, A. Bittar, G. V. M. Williams, J. E. Downes, A. DeMasi, Y. Zhang, K. E. Smith, and W. R. L. Lambrecht, Comparison between experiment and calculated band structures for DyN and SmN, Phys. Rev. B **76**, 245120 (2007).

[36] H. J. Trodahl, A. R. H. Preston, J. Zhong, B. J. Ruck, N. M. Strickland, C. Mitra, and W. R. L. Lambrecht, Ferromagnetic redshift of the optical gap in GdN, Phys. Rev. B **76**, 085211 (2007).

[37] R. Vidyasagar, T. Kita, T. Sakurai, and H. Ohta, Giant optical splitting in the spin-states assisting a sharp magnetic switching in GdN thin films, Appl. Phys. Lett. **102**, 222408 (2013).

[38] K. Senapati, M. G. Blamire, and Z. H. Barber, Spin-filter Josephson junctions, Nature Mater. **10**, 849 (2011).

[39] A. Kandala, A. Richardella, D. W. Rench, D. M. Zhang, T. C. Flanagan, and N. Samarth, Growth and characterization of hybrid insulating ferromagnet-topological insulator heterostructure devices, Appl. Phys. Lett. **103**, 202409 (2013).

[40] M. Azeem, Optical properties of rare earth nitrides, Ph.D. thesis, Victoria University of Wellington, 2013.

[41] C. Morari, F. Beiuşeanu, I. Di Marco, L. Peters, E. Burzo, S. Mican, and L. Chioncel, Magnetism and electronic structure

calculation of SmN, J. Phys.: Condens. Matter **27**, 115503 (2015).

[42] C.-M. Lee, H. Warring, S. Vézian, B. Damilano, S. Granville, M. Al Khalfioui, Y. Cordier, H. J. Trodahl, B. J. Ruck, and F. Natali, Highly resistive epitaxial Mg-doped GdN thin films, Appl. Phys. Lett. **106**, 022401 (2015).

[43] A. Punya, T. Cheiwchanchamnangij, A. Thiess, and Walter R. L. Lambrecht, First-principles study of nitrogen vacancies in GdN, in *MRS Proceedings*, Vol. 1290 (Cambridge University Press, Cambridge, UK, 2011).

[44] F. Leuenberger, A. Parge, W. Felsch, K. Fauth, and M. Hessler, GdN thin films: Bulk and local electronic and magnetic properties, Phys. Rev. B **72**, 014427 (2005).

[45] J. F. McNulty, B. J. Ruck, and H. J. Trodahl, On the ferromagnetic ground state of SmN, Phys. Rev. B **93**, 054413 (2016).

[46] C. Meyer, B. J. Ruck, J. Zhong, S. Granville, A. R. H. Preston, G. V. M. Williams, and H. J. Trodahl, Near-zero-moment ferromagnetism in the semiconductor SmN, Phys. Rev. B **78**, 174406 (2008).

[47] E.-M. Anton, B. J. Ruck, C. Meyer, F. Natali, H. Warring, F. Wilhelm, A. Rogalev, V. N. Antonov, and H. J. Trodahl, Spin/orbit moment imbalance in the near-zero moment ferromagnetic semiconductor SmN, Phys. Rev. B **87**, 134414 (2013).

[48] J. F. McNulty, E.-M. Anton, B. J. Ruck, F. Natali, H. Warring, F. Wilhelm, A. Rogalev, M. M. Soares, N. B. Brookes, and H. J. Trodahl, Twisted phase of the orbital-dominant ferromagnet SmN in a GdN/SmN heterostructure, Phys. Rev. B **91**, 174426 (2015).

[49] R. M. Moon and W. C. Koehler, Magnetic properties of SmN, J. Magn. Magn. Mater. **14**, 265 (1979).

[50] J. C. Parlebas, K. Asakura, A. Fujiwara, I. Harada, and A. Kotani, X-ray magnetic circular dichroism at rare-earth {L23} absorption edges in various compounds and alloys, Phys. Rep. **431**, 1 (2006).

[51] F. Natali, S. Vézian, S. Granville, B. Damilano, H. J. Trodahl, E.-M. Anton, H. Warring, F. Semond, Y. Cordier, S. V. Chong, and B. J. Ruck, Molecular beam epitaxy of ferromagnetic epitaxial GdN thin films, J. Cryst. Growth **404**, 146 (2014).

[52] A. Le Louarn, S. Vézian, F. Semond, and J. Massies, AlN buffer layer growth for GaN epitaxy on (111) Si: Al or N first? J. Cryst. Growth **311**, 3278 (2009).

[53] S. Granville, B. J. Ruck, F. Budde, A. Koo, D. J. Pringle, F. Kuchler, A. R. H. Preston, D. H. Housden, N. Lund, A. Bittar, G. V. M. Williams, and H. J. Trodahl, Semiconducting ground state of GdN thin films, Phys. Rev. B **73**, 235335 (2006).

[54] S. Yamanaka, K. Hotehama, and H. Kawaji, Superconductivity at 25.5 K in electron-doped layered hafnium nitride, Nature **392**, 580 (1998).

[55] B. W. Roberts, Survey of superconductive materials and critical evaluation of selected properties, J. Phys. Chem. Ref. Data **5**, 581 (1976).

[56] Y. Dubi, Y. Meir, and Y. Avishai, Nature of the superconductor–insulator transition in disordered superconductors, Nature **449**, 876 (2007).

[57] F. Natali, B. J. Ruck, H. J. Trodahl, D. L. Binh, S. Vézian, B. Damilano, Y. Cordier, F. Semond, and C. Meyer, Role of magnetic polarons in ferromagnetic GdN, Phys. Rev. B **87**, 035202 (2013).

[58] L. Pietronero, S. Strässler, and C. Grimaldi, Nonadiabatic superconductivity. I. Vertex corrections for the electron-phonon interactions, Phys. Rev. B **52**, 10516 (1995).

[59] S. Granville, C. Meyer, A. R. H. Preston, B. M. Ludbrook, B. J. Ruck, H. J. Trodahl, T. R. Paudel, and W. R. L. Lambrecht, Vibrational properties of rare-earth nitrides: Raman spectra and theory, Phys. Rev. B **79**, 054301 (2009).

[60] K. F. Garrity and D. Vanderbilt, Chern insulator at a magnetic rocksalt interface, Phys. Rev. B **90**, 121103 (2014).

[61] Z. Li, J. Kim, N. Kioussis, S.-Y. Ning, H. Su, T. Iitaka, T. Tohyama, X. Yang, and J.-X. Zhang, GdN thin film: Chern insulating state on square lattice, Phys. Rev. B **92**, 201303 (2015).